Univerzita Komenského v Bratislave

Fakulta matematiky, fyziky a informatiky

Mgr. Róbert Astaloš

Autoreferát dizertačnej práce

Bose-Einstein correlations in 7 TeV proton-proton collisions in the ATLAS experiment

na získanie akademického titulu philosophiae doctor

v odbore doktorandského štúdia:

4.1.5. Jadrová a subjadrová fyzika

Bratislava 2015

Dizertačná práca bola vypracovaná v dennej forme doktorandského štúdia na Katedre jadrovej fyziky Fakulty matematiky, fyziky a informatiky, Univerzity Komenského v Bratislave.

Predkladateľ: **Mgr. Róbert Astaloš**
Katedra jadrovej fyziky a biofyziky
Fakulta matematiky, fyziky a informatiky UK
842 48 Bratislava

Školitelia: **doc. RNDr. Stanislav Tokár, CSc.**
Katedra jadrovej fyziky a biofyziky FMFI UK, Bratislava

Prof. Dr. Nicolo de Groot
Univerzita Radboud v Nijmegene, Holandsko

Spoluškoliteľ: **Dr. Wesley Metzger**
Univerzita Radboud v Nijmegene, Holandsko

Oponenti:

1. **Prof. dr. S. J. de Jong**
   Univerzita Radboud v Nijmegene, Holandsko
2. **Prof. RNDr. Stanislav Vokál, DSc.**
   Univerzita Pavla Jozefa Šafárika v Košiciach
3. **Prof. E. Sarkisyan-Grinbaum**
   University of Texas at Arlington, USA

Obhajoba dizertačnej práce sa koná 30.09.2015 o 10:30 h

pred komisiou pre obhajobu dizertačnej práce v odbore doktorandského štúdia vymenovanou predsedom odborovej komisie .....

Študijný odbor: **4.1.5 Jadrová a subjadrová fyzika**, študijný program: **Jadrová a subjadrová fyzika**.

v Aule Univerzity Radboud, Comeniuslaan 2, 6525 HP Nijmegen, Holandsko

Predseda odborovej komisie:

prof. RNDr. Jozef Masarik, DrCs.
Katedra jadrovej fyziky a biofyziky
FMFI UK, 842 48 Bratislava

1 Bose-Einstein correlations

In this thesis, Bose-Einstein correlations (BEC) of like-sign charged boson pairs (mainly $\pi^{\pm}$) collected by the ATLAS experiment at the Large Hadron Collider (LHC) in 7TeV proton-proton collisions are analyzed in terms of various parametrizations: the wave function approach, the quantum optical approach and the τ model. The effect of BEC is experimentaly measured as a relative enhancement of the production of identical bosons with small 4-momentum differences, $Q = \sqrt{-(k_1 - k_2)^2}$, compared to the case without BEC. In order to see this enhancement, one constructs the correlation function $C_2(Q)$, which is the ratio of the two-particle probability density to the product of the single-particle densities.

The wave function (WF) approach assumes a two-boson wave function, which is symmetric under particle exchange, and chaotic particle emission. These two assumptions lead to the following forms of $C_2(Q)$ function (for different distributions of the source emission probability, which is assumed to be spherical in all cases):
$C_2(Q) = C_0 \left[1 + \lambda e^{-Q^2R^2}\right] (1 + \varepsilon Q)$ for a radial Gaussian distribution of the source,
$C_2(Q) = C_0 \left[1 + \lambda e^{-QR}\right] (1 + \varepsilon Q)$ for a radial Cauchy-Lorentz distribution of the source,
$C_2(Q) = C_0 \left[1 + \lambda e^{-(QR)^{\alpha}}\right] (1 + \varepsilon Q)$ for a symmetric Lévy parametrization of the source.
R is in each case a measure of the width of the corresponding source emission probability distribution representing a source size. λ (idealy equal to unity) is called the incoherence factor and is introduced to take into account a partially coherent source. Experimentally, the value of λ is also affected by other effects which reduce the amount of BEC, e.g., the presence of non-pions in the sample. The factors C_0 and $(1 + \varepsilon Q)$ are introduced in the fitting functions for the experimental data evaluation. C_0 is just a normalization constant, while $(1 + \varepsilon Q)$ is used to take into account long-distance correlations which are not included in these approaches (in the ideal case $\varepsilon = 0$).

The quantum optical (QO) approach assumes quantum statistics at high energies and high multiplicities where the conservation laws as well as the final state interactions can be neglected. It leads to the following forms of $C_2(Q)$ function (for different distributions of the source emission probability which is assumed to be spherical):
$C_2(Q) = C_0 \left[1 + 2p(1-p)e^{-R^2Q^2} + p^2 e^{-2R^2Q^2}\right] (1 + \varepsilon Q)$ for a Gaussian source distribution,
$C_2(Q) = C_0 \left[1 + 2p(1-p)e^{-RQ} + p^2 e^{-2RQ}\right] (1 + \varepsilon Q)$ for a Cauchy-Lorentz source distr.
R, C_0 and ε have the same interpretation as in the wave function approach. p is called chaoticity and is defined as the fraction of particles coming from the chaotic source. One can see, that the wave function approach $C_2(Q)$ functions are just particular cases of the quantum optical approach $C_2(Q)$ functions for $\lambda = p = 1$ as well as for $\lambda = p = 0$.

The τ model is inspired by the string picture of fragmentation. It assumes a particular form

for the time dependence of the particle emission. It leads to following form of $C_2(Q)$ function:

$$C_2(Q) = C_0 \left[1 + \lambda \cos\left(\tan\left(\tfrac{\pi\alpha}{2}\right)(QR)^{2\alpha}\right) e^{-(QR)^{2\alpha}}\right](1+\varepsilon Q).$$

This can be rewritten as

$$C_2(Q) = C_0 \left[1 + \lambda \cos\left(\quad (R_{\mathrm{a}}Q)^{2\alpha} \quad\right) e^{-(QR)^{2\alpha}}\right](1+\varepsilon Q),$$

and R_{a} can be used as a free parameter. This decouples, to some degree, the description of the anticorrelation region from that of the strong correlations around $Q = 0$. This additional degree of freedom can improve the fits. The parameters λ, C_0 and ε are introduced for the same reason as in the wave function approach. The R parameter is a width of a proper time distribution introduced by the time dependence of the particle emission.

2 LHC collider

To investigate the Bose-Einstein correlations described above, we use like-sign charged pion pairs produced in proton-proton collisions at the Large Hadron Collider (LHC) and detected by the ATLAS detector. The LHC is a proton-proton collider located at CERN (European Organization for Nuclear Research). The LHC is the largest, as well as most energetic, particle accelerator ever constructed. It is a synchrotron type of collider designed for pp collisions with center of mass energy up to 14 TeV. It has been installed in a 27 km long tunnel, 50 – 175 m below the ground, which had been used by the Large Electron-Positron collider (LEP) until 2000.

The protons at the LHC are accelerated in bunches. The data used in this thesis were taken at a center of mass energy of 7TeV, with 2 bunches of 0.76×10^{11} protons (one of them colliding in the ATLAS detector), the beam energy being ~ 86kJ.

3 ATLAS detector

The ATLAS detector is a multipurpose detector designed for a wide range of physics processes. As already mentioned, it takes data at the LHC. It was designed to gather data from both proton-proton and heavy ion collisions, however, its main focus is on protons. It has a cylindrical shape covering the whole space around the collision point. Reaching 46 m in length and 25 m in diameter, it is the largest volume particle detector ever constructed.

The resolutions of track transverse momentum p_{T}, azimuthal angle θ and polar angle ϕ measured by the ATLAS detector have been determined [1]. From these resolutions we can determine the resolution of the two particle 4-momentum difference Q, important for BEC studies. The resulting Q resolution is shown in Fig. 1, where the absolute and relative Q resolutions as a function

of Q are presented. We can see that for small Q values, the Q resolution is about 5MeV. With increasing Q the resolution of Q is also increasing and after Q = 600MeV the dependence becomes linear. At higher values of Q (> 600MeV) the relative resolution (σ_{Q}/Q) becomes saturated at a level of $\sim 2\%$. An important feature of σ_{Q} is that in the important interval for BEC its value does not exceed 20MeV.

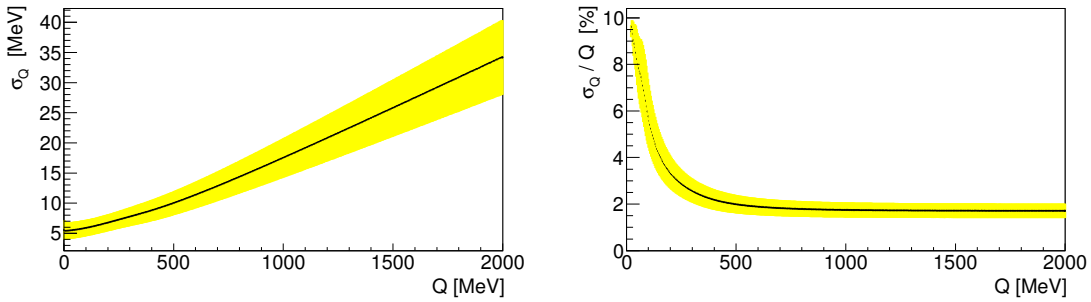

Figure 1: σ_{Q} as a function of Q (left) and the relative Q resolution, σ_{Q}/Q, as a function of Q (right) with $\pm 1\sigma$ bands.

4 Dataset

In the analysis, the minimum bias events accumulated in 2010 using the Minimum Bias Trigger Scintillators (MBTS) are used. The dataset consists of $\sim 10^7$ events which passed event selections. They contain $\sim 2.1 \times 10^8$ tracks in the pseudorapidity range $|\eta| < 2.5$ which passed the track selection criteria. This results in $\sim 1.8 \times 10^9$ like-sign charge track pairs.

Detection of particle tracks is subject to several effects, which can cause a track not to be detected or a fake track to appear. Therefore, several track corrections need to be introduced: track reconstruction efficiency, fraction of secondary particles, fraction of tracks outside of the kinematic range (the fraction of selected tracks passing the kinematic selection for which the corresponding primary particle is outside the kinematic range[1]), and fraction of fake tracks.

[1] because of the resolution effects, a track which is outside of the kinematic range is reconstructed as a track which passes the selection criteria

5 Reference distribution

Experimentally, the two-particle BEC correlation function $C_2(Q)$ is given by the ratio of the number of like-sign charged pairs $N(Q)$ in the data to the number of pairs in a reference sample, $N^{\mathrm{ref}}(Q)$. The reference sample should be identical to the signal sample except for the absence of Bose-Einstein correlations. We scale the $N^{\mathrm{ref}}(Q)$ distribution to have the same number of entries as the signal $N(Q)$ distribution to obtain a correct $C_2(Q)$ function.

For a reliable determination of the BEC effect it is critically important to have a correct reference distribution. Ideally, $N^{\mathrm{ref}}(Q)$ should have the same correlations as $N(Q)$ except for BEC. However, in practice, some compromise has to be made. To reduce any effects of additional correlations caused by a reference sample creating technique, the ratio of data and MC $C_2(Q)$ functions can be used:

$$R_2(Q) \;=\; \frac{C_2^{\mathrm{data}}(Q)}{C_2^{\mathrm{MC}}(Q)}. \tag{1}$$

Thus the denominator in $C_2(Q)$ function, $N^{\mathrm{ref}}(Q)$, is replaced by

$$N^{\mathrm{ref}}(Q) \cdot \frac{N_{\mathrm{MC}}(Q)}{N_{\mathrm{MC}}^{\mathrm{ref}}(Q)}, \tag{2}$$

which corrects $N^{\mathrm{ref}}(Q)$ for correlations (present in the MC distribution) which are removed or distorted by the method of the reference sample construction. If effects caused by the reference sample creating technique are comparable in data and MC distributions, they will cancel in their ratio. Thus the $R_2(Q)$ function can be more proper for the Bose-Einstein correlations studies than the $C_2(Q)$ function. We consider several different types of reference distribution:

i) **Unlike-sign pairs** (ULS). The reference distribution is constructed just like the signal distribution except that unlike-charged rather than like-charged tracks are used. Unlike-signed particles are not identical, thus in their two particle correlation distribution the BEC effect should not be present. However, its big disadvantage is the contribution of resonances to the unlike-sign charge two-particle distribution. To decrease the impact of resonances, the region of their biggest influence is excluded from the fit.

ii) **Event mixing** (MIX). The two tracks of the pair are taken from different events. The events are divided into groups according to their multiplicity ($n_{\mathrm{ch}} \in \langle 2,\,10\rangle$, $\langle 11,\,20\rangle$, $\langle 21,\,30\rangle$, $\langle 31,\,40\rangle$, $\langle 41,\,50\rangle$, $\langle 51,\,60\rangle$, $\langle 61,\,70\rangle$, $\langle 71,\,80\rangle$, $\langle 81,\,90\rangle$, $\langle 91,\,\infty\rangle$). Then each particle in a par-

ticular event is combined with every track of the same charge in the previous event in the same multiplicity interval. Thus tracks from each event are combined with tracks from two different events (the former one and the following one)[2]. This technique does not preserve any correlations of the original event, as the track pairs are created from different events.

iii) **Opposite hemisphere** (OHP). The momentum of one of the two tracks is inverted $(E, \vec{p}) \rightarrow (E, -\vec{p})$ before calculating the momentum difference Q of the pair. This technique preserves the energy of the original track pair.

iv) **Rotated track** (ROT). The momentum vector of one track of the pair is rotated by π about the beam direction, $(E, p_x, p_y, p_z) \rightarrow (E, -p_x, -p_y, p_z)$. This technique preserves the polar angle θ as well as the energy of the original track pair.

The unlike-sign pairs are not proper for use as a reference sample without corrections for the impact of resonances. The contribution of resonance decay products to data and MC samples is different, thus using the $R_2(Q)$ function is not sufficient for this correction.

The rotated track technique does not completely destroy the correlations in the signal sample, thus it is not proper for creating of a reference sample for the Bose-Einstein correlations studies.

Because of the prevalence of high Q values in the opposite hemisphere and event mixing reference samples, the $C_2(Q)$ functions with the reference samples created by the opposite hemisphere and event mixing techniques are not appropriate for the Bose-Einstein correlations studies. However, using the $R_2(Q)$ functions solves this problem. Thus the the $R_2(Q)$ functions with the reference samples created by the opposite hemisphere and event mixing techniques are both appropriate for the Bose-Einstein correlations studies.

Having no clear reason to choose between the event mixing and opposite hemisphere techniques, we have arbitrarily decided to use the opposite hemisphere technique as the main one for the studies presented in this thesis. On the other hand, there are some practical advantages of the opposite hemisphere technique like shorter time needed for computer calculations (one does not need to combine different events). Moreover, the mixing of events can be performed by several ways, thus the results are subject to the choice of mixing method, while inverting the track momentum is unambiguous.

[2]Except the very first event, which is combined only with the following one, and the very last event, which is combined only with the former one.

6 Results of fits of $R_2(Q)$ using the opposite hemisphere reference sample

The Bose-Einstein correlations studies performed using the opposite hemisphere reference sample are presented. The $R_2(Q)$ function (see Eq. 1) has been fitted by functions corresponding to three different parametrizations of the source emission probability in the wave function approach (WF): the Gaussian, the Lorentzian and the Lévy; as well two parametrizations of the quantum optical approach: the Gaussian and exponential. In addition, the τ model fits are presented. All the fits are carried out in the Q range of 20MeV – 2GeV. The region below 20MeV is excluded in order to avoid badly reconstructed or split tracks at very low Q values. Since for small Q values the Q resolution is about 5MeV and in the important interval for BEC the Q resolution does not exceed 20MeV (see the left plot of Fig. 1), this exclusion should be sufficient to avoid any problems of the detector resolution. For similar reasons, the bin width is chosen to be 20MeV. The upper Q boundary of the fit is chosen to be far away from the BEC sensitive region as well as far enough to determine the long-range correlations.

Results of the seven fits are shown in Fig. 2, and the fitted parameters are summarized in Tables 1 – 3. The χ^2 of the fits is also presented for the region of the BEC peak, the anticorrelation region and the tail separately. In each of these regions, the number of bins is stated rather than the number of degrees of freedom. The first region is chiefly responsible for determining R and λ (and α in the cases of the Lévy fit and τ model fit) whereas the other two regions are mainly responsible for determining C_0 and ε. Therefore it is reasonable to treat the peak region as ndf = bins-2 (ndf = bins-3 for the Lévy and τ model fits). For the other two regions, we can arbitrarily consider ndf = bins-1.

Looking at the figure and the tables one can see that none of the functions provides a good fit of the data. Of these, the Gaussian parametrization fits are by far the worst. The χ^2/ndf is more than three times higher than for the other parametrizations in both, the WF and QO approaches. Furthermore, most of the huge χ^2/ndf originates in the region of the BEC peak, which is most important for the BEC studies. It is interesting that Gaussian parametrizations of two different approaches (WF and QO) give very similar results (one can see only a tiny difference between the two functions for very small Q and the values of R agree). Further, one can see that the Lévy fitting parameter value $\alpha = 0.81$ is smaller than 1, thus the exponential fit is by all means preferred to the Gaussian one in WF. The $R_2(Q)$ correlation function decreases more steeply than allowed by the Gaussian and the exponential fits give much better descriptions of this behavior. The Lévy fit gives yet better agreement, as one sees in the magnified view of the BEC region in Fig. 2 as

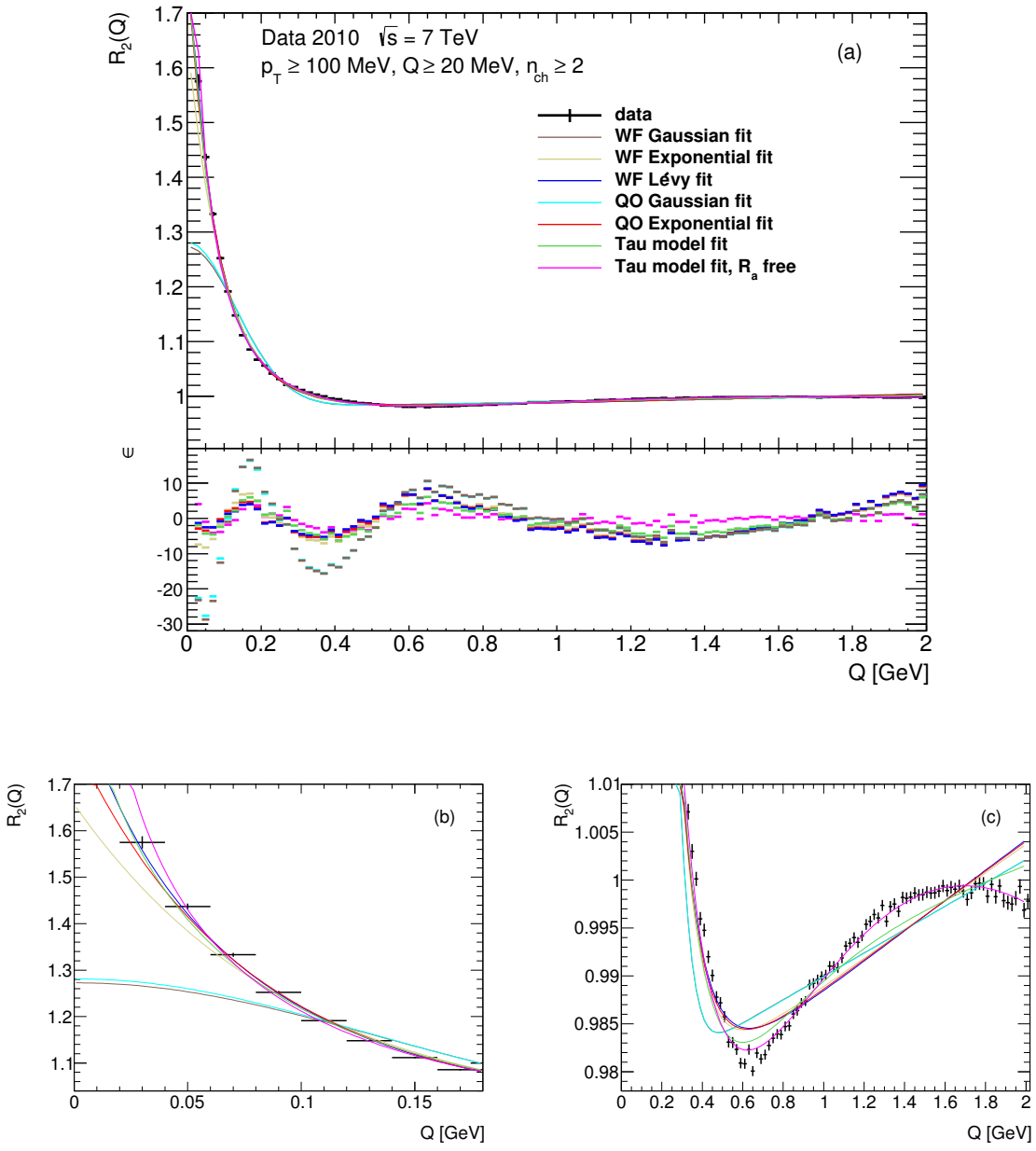

Figure 2: The $R_2(Q)$ correlation function with the opposite hemisphere like-sign pairs reference sample fitted by 7 fitting functions, three corresponding to different parametrizations of the source emission probability in the WF approach: the Gaussian, the exponential and the Lévy; two corresponding to parametrizations in the QO approach: the Gaussian and the exponential; and Tau model parametrizations (a) and details of the BEC peak region (b) and the anticorrelation part (c). The error bars represent the statistical uncertainties.

fit	Gaussian	Exponential	Lévy
α	$\equiv 2$	$\equiv 1$	0.81±0.01±0.18
C_0	0.9778±0.0002	0.9740±0.0002	0.9725±0.0003
λ	0.302±0.002±0.019	0.701±0.006±0.067	1.016±0.030±0.407
R [fm]	1.046±0.005±0.114	2.021±0.012±0.281	2.960±0.094±1.309
ε [GeV^{-1}]	0.0125±0.0002	0.0153±0.0002	0.0163±0.0002
χ^2/ndf	5932 / 95	1963 / 95	1755 / 94
χ^2/bins $(20 \leq Q \leq 360)$	3313 / 17	389 / 17	116 / 17
χ^2/bins $(360 \leq Q \leq 1600)$	2405 / 62	1175 / 62	1161 / 62
χ^2/bins $(1600 \leq Q \leq 2000)$	214 / 20	399 / 20	478 / 20

Table 1: The results of fits of the $R_2(Q)$ correlation function with the opposite hemisphere like-sign pairs reference sample with 3 fitting functions: the Gaussian, the exponential and the Lévy parametrizations of source emission probability in the wave function approach. The first (only) error shows the statistical uncertainty and the second error shows the systematic uncertainty.

fit	Gaussian	Exponential
C_0	0.9777±0.0002	0.9731±0.0002
p	0.169±0.002±0.012	0.606±0.013±0.106
R [fm]	1.032±0.005±0.112	1.779±0.006±0.185
ε [GeV^{-1}]	0.0125±0.0002	0.0159±0.0002
χ^2/ndf	5693 / 95	1737 / 95
χ^2/bins $(20 \leq Q \leq 360)$ [MeV]	3113 / 17	157 / 17
χ^2/bins $(360 \leq Q \leq 1600)$ [MeV]	2363 / 62	1135 / 62
χ^2/bins $(1600 \leq Q \leq 2000)$ [MeV]	217 / 20	445 / 20

Table 2: The results of fits of the $R_2(Q)$ correlation function with the opposite hemisphere like-sign pairs reference sample fitted by two parametrizations of the quantum optical approach: the Gaussian and the exponential. The first (only) error shows the statistical uncertainty and the second error shows the systematic uncertainty.

well as comparing the χ^2 values in the BEC peak region. However, the exponential fit has been used by most of the experiments. Therefore in the following, the exponential rather than the Lévy fit is considered the nominal one.

One can see that QO fits provide in general a slightly better description of the data than the WF fits. The χ^2/ndf is lower by 11.5% for the exponential parametrization. This is no dramatic difference and it can be expected, as the QO function is more general. On the other hand, the difference of χ^2 in the BEC peak region is huge. It is ∼2.5 times higher in the case of WF fit than in the QO case.

Although the χ^2/ndf is smaller for the exponential and Lévy fitting functions, its value is

fit	$R_{\rm a}$ fixed	$R_{\rm a}$ free
α	0.292±0.003±0.047	0.107±0.001±0.018
C_0	0.9872±0.0003	1.3349±0.0072
λ	1.200±0.035±0.529	3.162±0.037±0.774
R [fm]	3.45±0.12±2.05	19.03±0.63±9.51
ε [GeV^{-1}]	0.0074±0.0002	-0.0638±0.0004
$R_{\rm a}$ [fm]	-	24.1±1.1±12.0
$\chi^2/{\rm ndf}$	965 / 94	311 / 93
$\chi^2/{\rm bins}$ $(20 \leq Q \leq 360)$ [MeV]	186 / 17	115 / 17
$\chi^2/{\rm bins}$ $(360 \leq Q \leq 1600)$ [MeV]	600 / 62	177 / 62
$\chi^2/{\rm bins}$ $(1600 \leq Q \leq 2000)$ [MeV]	179 / 20	19 / 20

Table 3: The results of fits of the $R_2(Q)$ correlation function with the opposite hemisphere like-sign pairs reference sample fitted by the τ model functions. The first (only) error shows the statistical uncertainty and the second error shows the systematic uncertainty.

still too high. The main reason for the high $\chi^2/{\rm ndf}$ of the WF and QO parametrizations is their inability to describe the anticorrelation region around 0.5 – 1GeV as is seen in the blow-up of this region in Fig. 2. The τ model fit gives a better description of this region resulting in further improvement of the $\chi^2/{\rm ndf}$ (it is about half that of the exponential fits). However, the description is still inadequate and the $\chi^2/{\rm ndf}$ is too high. Further, the description of the BEC peak is better for the Lévy WF fitting function than for the τ model fit. Thus the advantage of the τ model is only in the description of the anticorrelation region and the tail. The τ model fit with $R_{\rm a}$ as a free parameter gives a further big improvement of $\chi^2/{\rm ndf}$. This improvement is chiefly due to a better description of the anticorrelation region and the tail. In fact it is the only function which can describe both the anticorrelation region and the tail reasonably well, while the description of the BEC peak is the same as in the case of the Lévy WF fitting function.

In the following sections, possible dependence of the BEC effect on track and kinematic observables (multiplicity, particle transverse momentum and transverse momentum of a particle pair) is investigated. For this purpose, the exponential parametrizations of WF and QO, the Lévy parametrization of WF and the τ model fit with $R_{\rm a}$ as a free parameter will be used.

7 Multiplicity dependence

In this section, the dependence of the fitting parameters on the charged particle multiplicity of the event is studied. The fits are performed and compared for 8 different multiplicity intervals.

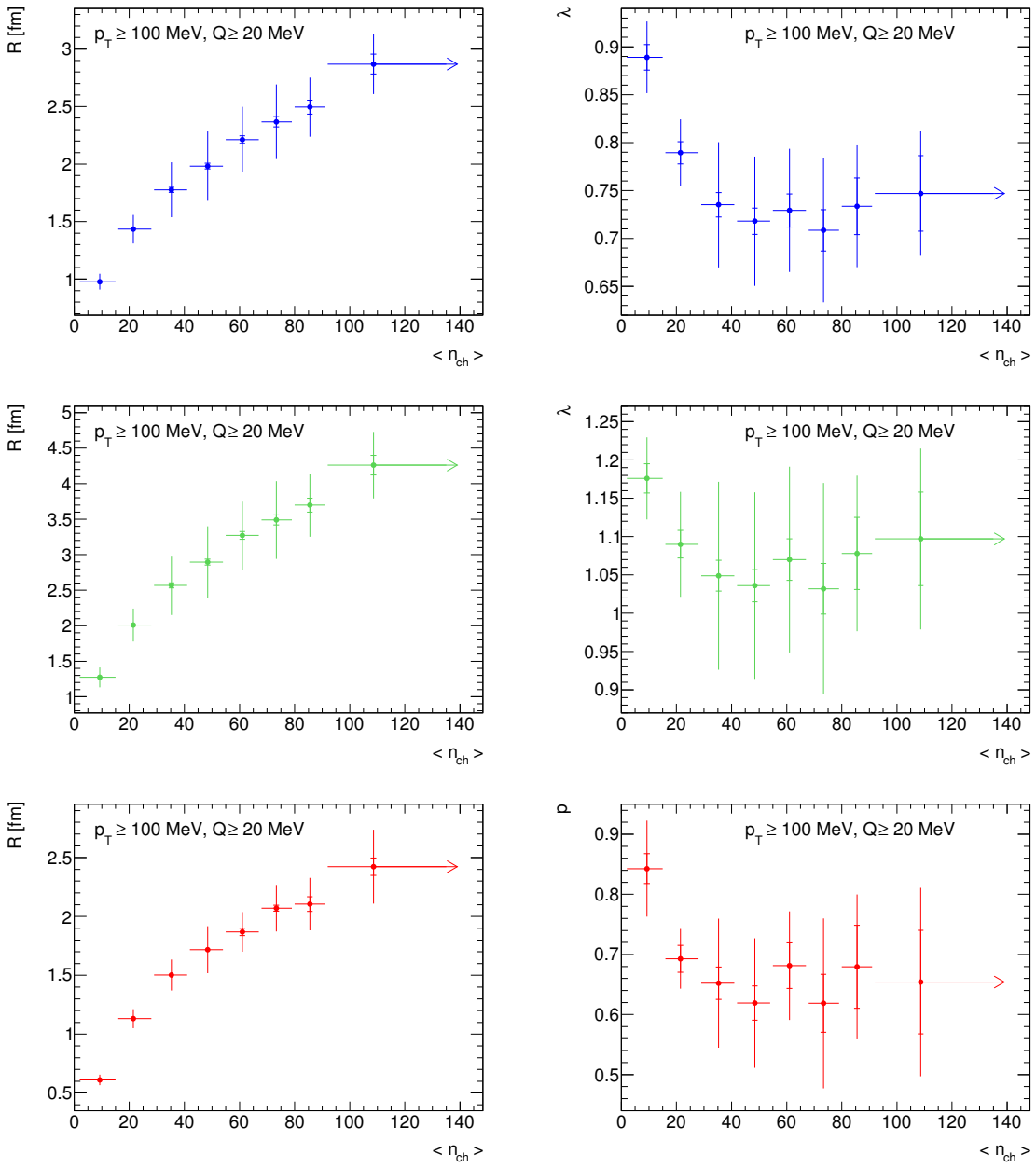

Figure 3: The $R_2(Q)$ function fit parameters R (left) and λ/p (right) from the wave function exponential (above) and Lévy (middle) parametrizations and the quantum optics exponential parametrization (below) as functions of track multiplicity obtained with opposite hemisphere reference samples. The vertical error bars represent both the statistical and the total uncertainties. The horizontal error bars represent the multiplicity intervals (the error bar margins show mean n_{ch} values corresponding to the margins of n_{sel} intervals).

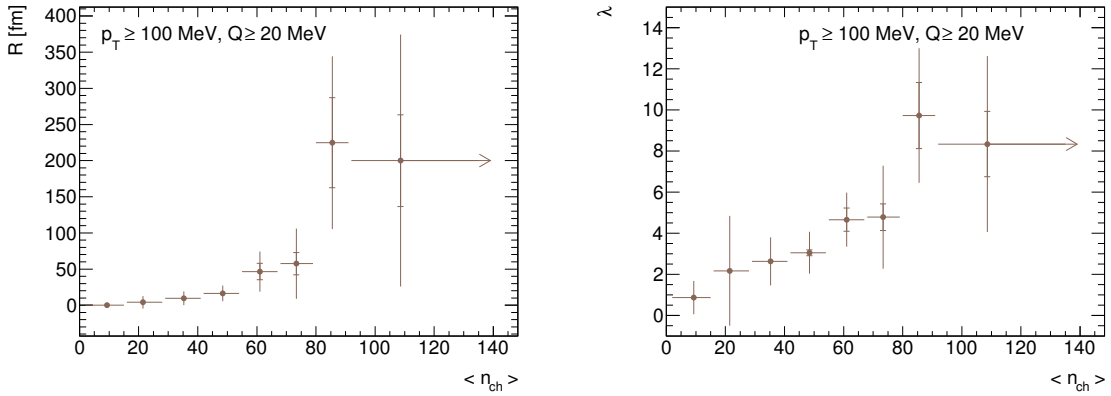

Figure 4: The $R_2(Q)$ function fit parameters R (left) and λ (right) from the τ model approach with $R_{\rm a}$ as a free parameter as functions of track multiplicity obtained with opposite hemisphere reference samples. The vertical error bars represent both the statistical and the total uncertainties. The horizontal error bars represent the multiplicity intervals (the error bar margins show mean $n_{\rm ch}$ values corresponding to the margins of $n_{\rm sel}$ intervals).

The fitted values of R and λ/p are shown as functions of the multiplicity in Fig. 3 and Fig. 4. One can see that the behavior of WF and QO fit functions is very similar. The radius R increases with the multiplicity. The λ and p clearly decrease with multiplicity for the low multiplicity intervals. They are consistent with being constant at high multiplicity, although the errors are too large to determine the exact behavior, and the statistical error bars can even cover a slightly decreasing behavior. It is very interesting that the behavior of R for all three functions is quite the same. Even the behavior of λ and p is similar in all rises and falls. The τ model fit parameters have a bit different behavior, which is expected as they have slightly different interpretation. Both R and λ clearly increase with multiplicity.

Similarly as in the case of multiplicity, R and λ show in general monotonic behavior also with transverse momentum of a track pair $k_{\rm T}$ and track transverse momentum $p_{\rm T}$ for all fitting functions (except the R dependence on $p_{\rm T}$ where one cannot make any strong conclusion).

8 Systematics and comparison of positively and negatively charged like-sign pairs

The leading source of systematic uncertainty is the use of the different Monte Carlo generators to correct the reference sample. The reason for that is that the Pythia6 MC generator does not reproduce the data very well. Another large source of systematic uncertainty is the upper Q boundary of

the fit. The higher the upper Q boundary (Q_{U}), the better the agreement of the WF exponential fit function with the BEC peak. In the case of the QO exponential fit, the description of the BEC peak improves when moving from $Q_{\mathrm{U}} = 2$GeV up to $Q_{\mathrm{U}} = 4$GeV, while it remains the same for higher Q_{U}. For the Lévy WF fit, there is no clear change in description of the BEC peak by moving to higher Q_{U}. For the τ model fit, the lower the upper Q boundary, the better the agreement with the BEC peak. The τ model with R_{a} as a free parameter is the only fit function which really follows the data, because it is able to describe the anticorrelation region. However, the χ^2/ndf is lower in the cases, when the anticorrelation region is excluded from fit (Lévy WF and QO exponential fits up to 5GeV). The description of the BEC peak is similar for the τ model and Lévy WF fits.

Because of the fact that the colliding particles are both positively charged, the momentum distributions of positively and negatively charged tracks differ in both the data and the MC samples. In general, the fit results for all like-sign pairs lie between the results for just positive or negative pairs, as expected. The R values are higher for negatively charged pairs.

9 Conclusions

A detailed study of the Bose-Einstein correlations of like-sign charged particles produced in 7TeV proton-proton collisions at the LHC and measured by the ATLAS detector in 2010 has been performed. Four reference samples have been tested. The sample of unlike-sign pairs is found to be greatly influenced by the decay products of resonances. The region of influence overlaps the BEC region, hence it cannot be completely excluded from the fit. The rotated track technique does not completely destroy correlations. Mixed events and opposite hemisphere techniques destroy correlations sufficiently, but they change the Q distribution resulting in a prevalence of high Q values. The correction by MC—use of R_2 instead of C_2—solves this problem. Both techniques have been found to work without any limitations for k_{T} up to 700MeV and p_{T} up to 500MeV and with some limitations for k_{T} and p_{T} up to 1000MeV. Of these two techniques, the opposite hemisphere has arbitrarily been chosen to provide the reference sample for the presented studies.

Several parametrizations have been used to fit the R_2 function with a reference sample created by the opposite hemisphere technique. However, none of them provides a good fit of the data. This disagreement is largely caused by the anticorrelation region, which the fit functions cannot follow. The only function which allows anticorrelations is the τ model fit. The anticorrelation region is also seen by the CMS experiment in 0.9 as well as 7TeV data [2].

The Gaussian parametrizations of WF as well as QO are by far the worst in description of the BEC peak. Further, the Lévy fitting parameter value $\alpha = 0.81$ is smaller than 1, thus the

exponential fit is by all means preferred to the Gaussian one in WF. The τ model fits improve the agreement of the function and data in the anticorrelation and tail regions, but do not improve the description of the BEC peak.

The exponential WF fit of the R_2 correlation function in the range 0.02 – 2GeV with the opposite hemisphere like-sign pairs reference sample gives the following results:

$$R = 2.02 \pm 0.01\ (\text{stat.}) \pm 0.28\ (\text{syst.})\ \text{fm}$$
$$\lambda = 0.701 \pm 0.006\ (\text{stat.}) \pm 0.067\ (\text{syst.})$$

These values are within systematic error in agreement with the values obtained for the same Q range by the CMS experiment using 7TeV data and a mixed-event reference sample [2]:

$$R_{\text{CMS}} = 1.89 \pm 0.02\ (\text{stat.}) \pm 0.19\ (\text{syst.})\ \text{fm}$$
$$\lambda_{\text{CMS}} = 0.618 \pm 0.009\ (\text{stat.}) \pm 0.039\ (\text{syst.})$$

The ALICE experiment has studied the dependence of R on n_{ch} and k_{T} at 7TeV using a mixed-event reference sample and Gaussian WF parametrization fit. It is expected that the result for the entire sample should be around the average of the results in intervals. Therefore, it makes sense to compare our result of the entire sample Gaussian WF fit with those obtained by ALICE for $n_{\text{ch}} \times k_{\text{T}}$ intervals. Our result is compatible within systematic error with results in 30 out of 48 $n_{\text{ch}} \times k_{\text{T}}$ intervals used by the ALICE [3].

The fitted values of R and λ/p of the exponential WF and QO parametrizations, the Lévy parametrization of WF and the τ model fit with R_{a} as a free parameter have also been studied as functions of the multiplicity, pair transverse momentum and hadron transverse momentum. It has been found that the radius R increases with the event multiplicity. The behavior of R for all WF and QO parametrizations is quite similar. Even the behavior of λ and p with multiplicity is similar in all rises and falls. Both λ and p clearly decrease with multiplicity for the low multiplicity intervals. They are consistent with being constant at high multiplicity, although the errors are too large to determine the exact behavior. The τ model fit parameters have a bit different behavior, which is expected as they have slightly different interpretation. Both R and λ clearly increase with multiplicity.

The monotonic behavior of R and λ with multiplicity was also confirmed using all of the other reference samples. It is in agreement with the results obtained by the CMS experiment [2], which has found that R increases and λ decreases with multiplicity, except for the interval of small k_{T}, where for the high multiplicity λ does not decrease. The same was found with earlier experiments

using $\mathrm{e^+e^-}$ collisions, by the OPAL experiment, which studied the multiplicity dependence up to $n_{\mathrm{ch}} = 40$ [4]. The increase of R with multiplicity in $\mathrm{e^+e^-}$ collisions is associated with an increase in the number of jets [5]. The E735 experiment studied the dependence of R and λ on the multiplicity at 1.8TeV $p\bar{p}$ data. It found, that values of the parameter R increase, while λ values decrease with multiplicity [6]. The ALICE experiment, in pp collisions, also finds that R increases with multiplicity for all k_{T} intervals (there are a few exceptions within errors) using 7TeV data with a mixed-event reference sample and a Gaussian WF parametrization fit [3]. The monotonic behavior of the fitting parameters with multiplicity has been predicted earlier and is an important ingredient of different models of multiparticle production [7–10].

Further, it has been found that the depth of the anticorrelation region is decreasing with multiplicity. The same behavior was found by the CMS experiment consistently for the two center of mass energies: 0.9 and 7TeV [2].

The R clearly increases and λ/p clearly decrease with k_{T} for all WF and QO parametrizations and their behavior is again similar. Both R and λ τ model fit parameters clearly increase with k_{T}.

λ/p clearly decrease with p_{T} for all WF and QO parametrizations, while one cannot make any strong conclusion about the behavior of the radius R with p_{T}. Both R and λ τ model fit parameters clearly decrease with p_{T}.

Because of the fact that the colliding particles are both positively charged, the momentum distributions of positively and negatively charged tracks differ in both the data and the MC samples. In general, the fit results for all like-sign pairs lie between the results for just positive or negative pairs, as expected. The R values are higher for negatively charged pairs.

The leading source of systematic uncertainty is the use of the different Monte Carlo generators for the R_2 function. The reason for that is that the Pythia6 MC generator does not reproduce the data very well. This systematic error could be reduced in future measurements by constraining different MC generators or their parameter settings from data.

Another large source of systematic uncertainty is the upper Q boundary of the fit. The higher the upper Q boundary, the better the agreement of the WF exponential fit function with the BEC peak. In the case of the QO exponential fit, the description of the BEC peak improves when moving from $Q_{\mathrm{U}} = 2$GeV up to $Q_{\mathrm{U}} = 4$GeV, while it remains the same for higher Q_{U}. For the Lévy WF fit, there is no clear change in description of the BEC peak by moving to higher Q_{U}. For the τ model fit, the lower the upper Q boundary, the better the agreement with the BEC peak. The τ model with R_{a} as a free parameter is the only fit function which really follows the data, because it is able to describe the anticorrelation region. However, the χ^2/ndf is lower in the cases, when the anticorrelation region is excluded from fit (Lévy WF and QO exponential fits up to 5GeV). The

description of the BEC peak is similar for τ model and Lévy WF fits. In future measurements, better fits could be obtained by adding an anticorrelation term to the WF and QO fit functions or by excluding the anticorrelation region systematically.

The behavior of the unlike-sign pairs reference sample differs very much from the other reference samples. Among the other reference samples, the values for the rotated track reference sample differ in general from the opposite hemisphere and mixed events reference samples. The latter two are in most cases similar.

10 Publications

[I] ATLAS Collaboration, G. Aad et al., *Measurement of the differential cross-section of B+ meson production in pp collisions at* $\sqrt{s} = 7$ *TeV at ATLAS*, Journal of High Energy Physics. - No. 10 (2013), Art. No. 042, s. 1-37.

[II] ATLAS Collaboration, G. Aad et al., *Measurement with the ATLAS detector of multi-particle azimuthal correlations in p plus Pb collisions at* $\sqrt{s}(NN) = 5.02$ *TeV*, Physics Letters B. - Vol. 725, No. 1-3 (2013), s. 60-78.

[III] ATLAS Collaboration, G. Aad et al., *Search for long-lived stopped R-hadrons decaying out of time with pp collisions using the ATLAS detector*, Physical Review D. - Vol. 88, No. 11 (2013), Art. No. 112003, s. 1-30.

[IV] ATLAS Collaboration, G. Aad et al., *Measurement of the azimuthal angle dependence of inclusive jet yields in Pb plus Pb collisions at* $\sqrt{s}(NN) = 2.76$ *TeV with the ATLAS detector*, Physical Review Letters. - Vol. 111, No. 15 (2013), Art. No. 152301, s. 1-18.

[V] ATLAS Collaboration, G. Aad et al., *Performance of jet substructure techniques for large-R jets in proton-proton collisions at* $\sqrt{s} = 7$ *TeV using the ATLAS detector*, Journal of High Energy Physics. - No. 9 (2013), Art. No. 076, s. 1-81.

[VI] ATLAS Collaboration, G. Aad et al., *Dynamics of isolated-photon plus jet production in pp collisions at* $\sqrt{s} = 7$ *TeV with the ATLAS detector*, Nuclear Physics B. - Vol. 875, No. 3 (2013), s. 483-535.

[VII] ATLAS Collaboration, G. Aad et al., *The differential production cross section of the phi(1020) meson in $\sqrt{s} = 7$ TeV pp collisions measured with the ATLAS detector*, The European Physical Journal C - Particles and Fields. - Vol. 74, No. 7 (2014), Art. No. 2895, s. 1-21.

[VIII] ATLAS Collaboration, G. Aad et al., *Measurement of the cross-section of high transverse momentum vector bosons reconstructed as single jets and studies of jet substructure in pp collisions at $\sqrt{s} = 7$ TeV with the ATLAS detector*, New Journal of Physics. - Vol. 16, No. (2014), Art. No. 113013, s. 1-34.

[IX] ATLAS Collaboration, G. Aad et al., *Measurementof the inclusive isolated prompt photons cross section in pp collisions at $\sqrt{s} = 7$ TeV with the ATLAS detector using 4.6 fb(-1)*, Physical Review D. - Vol. 89, No. 5 (2014), Art. No. 052004, s. 1-24.

[X] ATLAS Collaboration, G. Aad et al., *Measurement of dijet cross-sections in pp collisions at 7 TeV centre-of-mass energy using the ATLAS detector*, Journal of High Energy Physics. - No. 5 (2014), Art. No. 059, s. 1-66.

[XI] ATLAS Collaboration, G. Aad et al., *Measurement of the underlying event in jet events from 7 TeV proton-proton collisions with the ATLAS detector*, The European Physical Journal C - Particles and Fields. - Vol. 74, No. 8 (2014), Art. No. 2965, s. 1-29.

[XII] ATLAS Collaboration, G. Aad et al., *Measurement of distributions sensitive to the underlying event in inclusive Z-boson production in pp collisions at $\sqrt{s} = 7$ TeV with the ATLAS detector*, The European Physical Journal C - Particles and Fields. - Vol. 74, No. 12 (2014), Art. No. 3195, s. 1-33.

[XIII] ATLAS Collaboration, G. Aad et al., *Measurements of jet vetoes and azimuthal decorrelations in dijet events produced in pp collisions at $\sqrt{s} = 7$ TeV using the ATLAS detector*, The European Physical Journal C - Particles and Fields. - Vol. 74, No. 11 (2014), Art. No. 3117, s. 1-27.

[XIV] ATLAS Collaboration, G. Aad et al., *Jet energy measurement and its systematic uncertainty in proton-proton collisions at $\sqrt{s} = 7$ TeV with the ATLAS detector*, The European Physical Journal C - Particles and Fields. - Vol. 75, No. 1 (2015), Art. No. 17, s. 1-101.

Publication sent to journal

ATLAS Collaboration, G. Aad et al., *Two-particle Bose-Einstein correlations in pp collisions at $\sqrt{s} = 0.9$ and 7 TeV measured with the ATLAS detector*, arXiv:1502.07947 - submitted to EPJC.

References

[1] ATLAS Collaboration, CERN-OPEN-2008-020 (Chapt. Performance, Sec.Tracking), December 2008.

[2] CMS Collaboration, V. Khachatryan et al., JHEP 05 (2011) 029.

[3] ALICE Collaboration, K. Aamodt et al., Phys. Rev. D 84 (2011) 112004.

[4] OPAL Collaboration, G. Alexander et al., Z. Phys. C 72 (1996) 389.

[5] G. Alexander, J. Phys. G 39 (2012) 085007.

[6] T. Alexopoulos et al., Phys.Rev. D48, 1931 (1993).

[7] W. Kittel, E.A. De Wolf, *Soft Multihadron Dynamics*, World Scientific, Singapore (2005).

[8] N. Suzuki, M. Biyajima, Phys. Rev. C 60 (1999) 034903.

[9] B. Buschbeck, H.C. Eggers, P. Lipa, Phys. Lett. B 481 (2000) 187.

[10] G. Alexander, E.K.G. Sarkisyan, Phys. Lett. B 487 (2000) 215.